

# Synthesis, Structural Studies, and Physical Properties of the $RE_5Mo_{32}O_{54}$ ( $RE = La, Ce, Pr, Nd$ ) Compounds Containing *trans*-Bicapped $Mo_8$ Octahedral Clusters and $Mo_7$ – $Mo_{10}$ – $Mo_7$ Triclusters

J. Tortelier, P. Gall,\* H. Noël, and P. Gougeon<sup>1</sup>

Laboratoire de Chimie du Solide et Inorganique Moléculaire, UMR CNRS 6511, Université de Rennes I, Avenue du Général Leclerc, 35042 Rennes cedex, France; and \*Laboratoire de Chimie des Matériaux Inorganiques et de Cristallographie, 20 av des buttes de Coesmes, 35043 Rennes cedex, France

Received October 21, 1999; in revised form February 22, 2000; accepted March 3, 2000

**Polycrystalline samples and single crystals of the  $RE_5Mo_{32}O_{54}$  compounds ( $R = La, Ce, Pr$ , and  $Nd$ ) were synthesized by solid state reactions at high temperature in sealed Mo crucibles. Their crystal structures were determined by single crystal X-ray diffraction methods. All four compounds are isostructural and crystallize in the monoclinic  $P2_1/c$  space group. Their crystal structure exhibits two different cluster types: an isolated bicapped octahedral  $Mo_8$  cluster having an isomeric *trans* form and a  $Mo_{24}$  chain fragment that can be described as  $Mo_7$ – $Mo_{10}$ – $Mo_7$  triclusters. The oxygen atoms bridge all Mo–Mo edges or are linked to free apices. Both  $Mo_8O_{24}$  and  $Mo_{24}O_{60}$  cluster units are arranged in layers parallel to the *ac* plane. These compounds show semiconducting behavior with activation energies of about 0.06 eV and room temperature resistivities in the range 0.04–0.08  $\Omega \cdot cm$ . The magnetic susceptibility data reveal a magnetic moment of  $1.77 \mu_B$  localized on the Mo sublattice in addition to that arising from the rare-earth ions.** © 2000 Academic Press

**Key Words:** oxides; cluster; molybdenum; electrical properties; magnetic properties.

## INTRODUCTION

High-nucularity molybdenum clusters in solid state compounds result principally from the uniaxial *trans*-face or -edge sharing of octahedral  $Mo_6$  clusters. The former process is observed when the  $Mo_6$  clusters are face-bridged by the ligands (S, Se, and Te) and is exemplified, in particular, by the series of compounds  $M_{n-2}Mo_{3n}X_{3n+2}$  ( $M = Rb, Cs$ ;  $X = S, Se$  or  $Te$ ;  $n = 3, 4, 5, 6, 7, 8, 10$ , and 12) containing  $Mo_{3n}$  clusters (1–5). The final stage of this face-sharing

condensation is the infinite  $|Mo_{6/2}|_\infty^1$  chain found in the quasi-one-dimensional compounds  $M_2Mo_6X_6$  ( $M = Na, K, Rb, Cs$ ;  $X = S, Se$ , or  $Te$ ) (8) and  $AgMo_6Te_6$  (9). The edge-sharing condensation of  $Mo_6$  octahedra is observed in reduced molybdenum oxides, where the  $Mo_6$  clusters are edge-bridged by the oxygen atoms. This process leads to  $Mo_{4n+2}$  oligomers that are observed for example in the series  $M_{n-x}Mo_{4n+2}O_{6n+4}$  ( $n = 2, 3, 4$ , and 5) (10–13). The ultimate step of the edge-sharing-condensation process corresponds to the infinite  $|Mo_2Mo_{4/2}|_\infty^1$  chain of *trans*-edge-sharing  $Mo_6$  octahedra that was first observed in  $NaMo_4O_6$  (14). More recently, two original high-nucularity molybdenum clusters, i.e.,  $Mo_{19}$  and  $Mo_{24}$ , were observed in reduced molybdenum oxides. The first one results from a three-dimensional edge-sharing of  $Mo_6$  octahedra and was found in the atypical compound  $Pr_4Mo_9O_{18}$  (15). The second one is built up from one  $Mo_{10}$  and two  $Mo_7$  clusters interconnected through short Mo–Mo bonds of about 2.77 Å and was observed in coexistence with bicapped octahedral  $Mo_8$  clusters in  $La_5Mo_{32}O_{54}$  (16). The trilcluster  $Mo_7$ – $Mo_{10}$ – $Mo_7$  thus formed also constitutes the repeat unit of the infinite chain found in the quaternary  $M_4M'_3Mo_{26}O_{48}$  ( $M = Sr, Eu$ ;  $M' = Al, Fe, Ga$ ) compounds (17, 18). The interest of this class of compounds with high nucularity Mo clusters not only resides in their fascinating structural aspects but also in the various electrical and magnetic properties they exhibit. For example, the sulfides and selenides are usually superconductors at low temperature (19). Up to now, no superconductivity has been observed in the molybdenum cluster oxides. However, the latter compounds often present a metal–insulator transition (20) or unusual resistivity behaviors (21) as well as various magnetic behaviors (22). This paper deals with the synthesis, crystal growth, and physical and electrical properties of  $La_5Mo_{32}O_{54}$  and the new isostructural  $Ce$ ,  $Pr$ , and  $Nd$  compounds.

\*To whom correspondence should be addressed. Fax: (33) 2.99.63.57.04. E-mail: patrick.gougeon@univ-rennes1.fr.



## EXPERIMENTAL

**Synthesis.** The starting reagents were  $\text{La}_2\text{O}_3$ ,  $\text{CeO}_2$ ,  $\text{Pr}_6\text{O}_{11}$ ,  $\text{Nd}_2\text{O}_3$  (Strem Chemicals, 99.999%),  $\text{MoO}_3$  (Strem Chemicals, 99.9%), and Mo, all in powder form. Before use the Mo powder was heated under a hydrogen flow at 1000°C for 6 h and the rare-earth oxides were prefired at temperatures between 700 and 1000°C overnight and left at 600°C before weighing them. All reactions were done in molybdenum crucibles (depth, 2.5 cm; diam, 1.5 cm) that had previously been outgassed at about 1500°C for 15 min under a dynamic vacuum of about  $10^{-5}$  Torr. For each compound, the correct stoichiometry mole ratio of the starting reagents was ground, pressed into pellet (ca. 5 g), and loaded into a molybdenum crucible which was then sealed under a low argon pressure using an arc welding system. Pure X-ray powders were synthesized after heating at 1600°C for 48 h and single crystals were obtained by heating compositions  $\text{REMo}_6\text{O}_{12}$  (Ce, Nd) or  $\text{RE}_6\text{Mo}_{31.5}\text{O}_{62.5}$  (Pr) at 2000°C for 5 min. In both cases, the crucibles were then cooled at a rate of  $100^\circ\text{C}\text{h}^{-1}$  to 1100°C, at which temperature the furnace was shut off. Attempts to synthesize isostructural compounds with smaller or divalent rare-earths (Sm, Eu, Gd) were not successful and the final major product was found to be  $\text{REMo}_5\text{O}_8$  (22).

**Single crystal X-ray studies.** Single crystals of the Ce, Pr, and Nd members were selected for X-ray structure determinations. The intensity data were collected on a CAD4 Enraf-Nonius diffractometer using a graphite-monochromatized  $\text{MoK}\alpha$  radiation ( $\lambda = 0.71073 \text{ \AA}$ ) at 20°C. The lattice constants were determined by least squares refinement of the setting angles of 25 reflections in the  $\theta$  range 6.5–23.5° that had been automatically centered on the diffractometer. For each crystal, three standard reflections were measured every 90 min and showed no significant variation in intensity during data collection. The intensity data sets were corrected for Lorentz and polarization effects and empirical absorptions were applied based upon azimuthal scans of nine reflections (23). The three structures were refined in the space group  $P2_1/c$ . Positional parameters of  $\text{La}_5\text{Mo}_{32}\text{O}_{54}$  (16) were used in the first stages of the refinements. The final refinement cycles included the atomic coordinates, anisotropic displacement parameters for rare-earth and Mo atoms. Calculations were performed on a Digital microVAX 3100 using the MolEN (24) package. The lattice parameters and the details of the X-ray single data collections and structure refinements for the three compounds investigated are summarized in Table 1. Final positional and equivalent isotropic displacement parameters are listed in Tables 2, 3, and 4. Selected

TABLE 1  
Crystallographic and Experimental Data for  $\text{RE}_5\text{Mo}_{32}\text{O}_{54}$  (RE = Ce, Pr, Nd)

Compound	$\text{Ce}_5\text{Mo}_{32}\text{O}_{54}$	$\text{Pr}_5\text{Mo}_{32}\text{O}_{54}$	$\text{Nd}_5\text{Mo}_{32}\text{O}_{54}$
Crystal system		Monoclinic	
Space group		$P2_1/c$	
$a$ (Å)	10.183(2)	10.177(2)	10.16(1)
$b$ (Å)	9.1328(8)	9.1171(5)	9.115(4)
$c$ (Å)	22.905(4)	22.880(3)	22.85(1)
$\beta$ (°)	105.207(9)	105.186(6)	105.28(2)
$V$ (Å <sup>3</sup> )	2055.7(6)	2049.0(3)	2042(2)
Molecular weight (g mol <sup>-1</sup> )	4634.65	4638.58	4655.25
Z, density (calc., g cm <sup>-3</sup> )	2; 7.487	2; 7.514	2; 7.568
Crystal color, morphology	Black, irregular	Black, irregular	Black, irregular
Crystal size (mm <sup>3</sup> )	0.1 × 0.1 × 0.08	0.2 × 0.08 × 0.04	0.16 × 0.1 × 0.1
Linear absorption coeff. (mm <sup>-1</sup> )	14.80	15.12	15.61
2 $\theta$ recording range (°)	2/60	2/64	2/60
$h, k, l$ range	0/14, 0/12, -32/32	0/15, 0/13, -34/34	0/14, 0/12, -32/32
No. of measured reflections	6615	7849	6576
No. of independent reflections	5109	6771	5345
No. of observed reflections with $F_o^2 > 2\sigma(F_o^2)$	3675	5917	3998
No. of refined parameters	278	278	198
$R_{\text{int}}$	0.032	0.023	0.041
Absorption correction type	Ψ Scan	Ψ Scan	Ψ Scan
Transmission (min.; max.)	0.248; 0.306	0.429; 0.546	0.177; 0.210
Refinement on	$F$	$F$	$F$
$R[F_o^2 > 2\sigma(F_o^2)]$	0.0352	0.0309	0.0450
$Rw$ with $w = 4F_o^2/[\sigma^2(F_o^2) + (0.04F_o^2)^2]$	0.0477	0.0515	0.0543
Extinction coefficient	$3.3(1) \times 10^{-8}$	$3.5(1) \times 10^{-8}$	$2.06(1) \times 10^{-7}$
$S$	1.267	1.699	1.601
Residuals ( $e^-/\text{\AA}^3$ ) max.; min.	2.27, -1.52	2.02, -0.77	3.90, -1.17
$\Delta/\sigma_{\text{max}}$	< 0.01	< 0.01	< 0.01

**TABLE 2**  
**Fractional Atomic Coordinates and Isotropic or Equivalent-Isotropic Displacement Parameters ( $\text{\AA}^2$ ) for  $\text{Ce}_5\text{Mo}_{32}\text{O}_{54}$**

Atom	x	y	z	( $\text{\AA}^2$ )
Ce1	0.000	0.000	0.500	0.53(2)
Ce2	0.23290(7)	0.99518(9)	0.20604(3)	0.66(1)
Ce3	0.47413(7)	0.00428(9)	0.08024(3)	0.51(1)
Mo1	0.8453(1)	0.1204(1)	0.09643(5)	0.23(2)
Mo2	0.91314(9)	0.6177(1)	0.55189(4)	0.21(2)
Mo3	0.07878(9)	0.1248(1)	0.06822(4)	0.24(2)
Mo4	0.1577(1)	0.8778(1)	0.02126(5)	0.26(2)
Mo5	0.93576(9)	0.8767(1)	0.67709(4)	0.23(2)
Mo6	0.15688(9)	0.8766(1)	0.76690(4)	0.20(2)
Mo7	0.31921(9)	0.1196(1)	0.78802(4)	0.24(2)
Mo8	0.91933(9)	0.8784(1)	0.30312(4)	0.22(2)
Mo9	0.40529(9)	0.8783(1)	0.74179(4)	0.23(2)
Mo10	0.83649(9)	0.1221(1)	0.35028(4)	0.21(2)
Mo11	0.66697(9)	0.8850(1)	0.32957(4)	0.21(2)
Mo12	0.42484(9)	0.8845(1)	0.61297(4)	0.19(2)
Mo13	0.5949(1)	0.1130(1)	0.63007(4)	0.22(2)
Mo14	0.34693(9)	0.1277(1)	0.53839(4)	0.21(2)
Mo15	0.34030(9)	0.1340(1)	0.42483(4)	0.21(2)
Mo16	0.41403(9)	0.8749(1)	0.49066(4)	0.22(2)
O1	0.3336(8)	0.754(1)	0.9173(4)	0.4(1)
O2	0.2508(8)	0.995(1)	0.8448(3)	0.4(1)
O3	0.0812(8)	0.761(1)	0.8260(4)	0.6(1)
O4	0.8335(8)	0.748(1)	0.1042(4)	0.5(1)
O5	0.0172(7)	0.993(1)	0.1280(3)	0.3(1)
O6	0.1732(8)	0.2597(9)	0.6494(4)	0.3(1)
O7	0.2707(7)	0.500(1)	0.4759(3)	0.3(1)
O8	0.0765(8)	0.768(1)	0.4544(4)	0.7(1)
O9	0.9243(8)	0.264(1)	0.9284(4)	0.6(1)
O10	0.2525(8)	0.498(1)	0.5964(4)	0.4(1)
O11	0.8333(8)	0.7399(9)	0.9817(4)	0.3(1)
O12	0.3392(8)	0.7415(9)	0.5458(4)	0.2(1)
O13	0.2465(8)	0.010(1)	0.3477(4)	0.4(1)
O14	0.8332(8)	0.741(1)	0.2317(4)	0.4(1)
O15	0.0952(8)	0.770(1)	0.1987(4)	0.3(1)
O16	0.9975(8)	0.992(1)	0.3822(4)	0.4(1)
O17	0.0150(7)	0.993(1)	0.2477(3)	0.2(1)
O18	0.3376(8)	0.750(1)	0.1681(4)	0.4(1)
O19	0.3238(8)	0.740(1)	0.7887(4)	0.3(1)
O20	0.4114(8)	0.248(1)	0.2395(4)	0.3(1)
O21	0.5216(8)	0.997(1)	0.6943(4)	0.4(1)
O22	0.4932(8)	0.001(1)	0.8112(4)	0.4(1)
O23	0.7594(7)	0.997(1)	0.4114(3)	0.3(1)
O24	0.5721(8)	0.744(1)	0.8832(4)	0.4(1)
O25	0.5829(8)	0.766(1)	0.1310(4)	0.4(1)
O26	0.2406(8)	0.995(1)	0.4715(4)	0.4(1)
O27	0.5643(8)	0.782(1)	0.0052(4)	0.5(1)

interatomic distances are given in Tables 5, 6, and 7 and compared to those observed for the previously published compound  $\text{La}_5\text{Mo}_{32}\text{O}_{54}$  ( $a = 10.176(2)$   $\text{\AA}$ ,  $b = 9.1471(5)$   $\text{\AA}$ ,  $c = 22.910(3)$   $\text{\AA}$ ,  $\beta = 105.136(7)^\circ$ , and  $V = 2058.6(4)$   $\text{\AA}^3$ ).

*Electrical conductivity and magnetic susceptibility measurements.* The ac resistivity measurements were performed on single crystals of  $\text{La}_5\text{Mo}_{32}\text{O}_{54}$ ,  $\text{Ce}_5\text{Mo}_{32}\text{O}_{54}$ ,

$\text{Pr}_5\text{Mo}_{32}\text{O}_{54}$ , and  $\text{Nd}_5\text{Mo}_{32}\text{O}_{54}$  with currents of 1 mA, using a standard four-probe technique between 300 and 80 K. Ohmic contacts were made by attaching molten indium ultrasonically. The magnetic susceptibility data of cold-pressed pellets (ca. 150 mg) were recorded using SHE SQUID magnetometer in the temperature range 2–300 K with an applied field of 2 kG.

**TABLE 3**  
**Fractional Atomic Coordinates and Isotropic or Equivalent-Isotropic Displacement Parameters ( $\text{\AA}^2$ ) for  $\text{Pr}_5\text{Mo}_{32}\text{O}_{54}$**

Atom	x	y	z	( $\text{\AA}^2$ )
Pr1	0.000	0.000	0.500	0.539(2)
Pr2	0.23108(4)	0.99448(5)	0.20544(2)	0.688(6)
Pr3	0.47170(4)	0.00412(4)	0.08045(2)	0.523(6)
Mo1	0.84530(5)	0.12067(6)	0.09631(2)	0.204(8)
Mo2	0.91313(5)	0.61819(6)	0.55176(2)	0.172(8)
Mo3	0.07877(5)	0.12465(8)	0.06837(2)	0.186(8)
Mo4	0.15724(5)	0.87746(6)	0.02120(2)	0.214(8)
Mo5	0.93576(5)	0.87707(6)	0.67704(2)	0.205(8)
Mo6	0.15693(5)	0.87636(6)	0.76698(2)	0.181(8)
Mo7	0.31940(5)	0.11939(6)	0.78825(2)	0.194(8)
Mo8	0.91922(5)	0.87814(6)	0.30308(2)	0.194(8)
Mo9	0.40548(5)	0.87794(6)	0.74186(2)	0.200(8)
Mo10	0.83633(5)	0.12158(6)	0.35036(2)	0.179(8)
Mo11	0.66680(5)	0.88474(6)	0.32957(2)	0.168(8)
Mo12	0.42474(5)	0.88427(6)	0.61301(2)	0.181(8)
Mo13	0.59497(5)	0.11286(6)	0.63015(2)	0.199(8)
Mo14	0.34707(5)	0.12760(6)	0.53845(2)	0.171(8)
Mo15	0.34035(5)	0.13433(6)	0.42497(2)	0.195(8)
Mo16	0.41406(5)	0.87479(6)	0.49064(2)	0.187(8)
O1	0.3335(5)	0.7563(6)	0.9173(2)	0.43(7)
O2	0.2501(5)	0.9963(6)	0.8452(2)	0.42(7)
O3	0.0826(4)	0.7594(5)	0.8266(2)	0.25(6)
O4	0.8340(4)	0.7472(6)	0.1039(2)	0.28(6)
O5	0.0164(5)	0.9943(5)	0.1281(2)	0.26(6)
O6	0.1739(5)	0.2610(6)	0.6495(2)	0.49(7)
O7	0.2702(5)	0.4985(5)	0.4761(2)	0.38(7)
O8	0.0770(4)	0.7701(6)	0.4548(2)	0.36(7)
O9	0.9240(5)	0.2628(6)	0.9291(2)	0.53(7)
O10	0.2521(5)	0.4997(5)	0.5963(2)	0.33(7)
O11	0.8351(4)	0.7384(6)	0.9826(2)	0.38(7)
O12	0.3411(4)	0.7405(5)	0.5462(2)	0.25(6)
O13	0.2469(5)	0.0091(5)	0.3484(2)	0.23(6)
O14	0.8347(5)	0.7391(6)	0.2308(2)	0.55(7)
O15	0.0963(5)	0.7731(5)	0.1995(2)	0.34(7)
O16	0.9969(5)	0.9918(5)	0.3822(2)	0.37(7)
O17	0.0129(5)	0.9922(6)	0.2472(2)	0.35(7)
O18	0.3375(5)	0.7519(6)	0.1687(2)	0.46(7)
O19	0.3245(5)	0.7381(6)	0.7879(2)	0.45(7)
O20	0.4106(4)	0.2479(6)	0.2394(2)	0.40(7)
O21	0.5209(5)	0.9980(5)	0.6944(2)	0.35(7)
O22	0.4931(5)	−0.0015(5)	0.8110(2)	0.41(7)
O23	0.7589(5)	0.9966(5)	0.4117(2)	0.35(7)
O24	0.5722(4)	0.7471(6)	0.8834(2)	0.35(7)
O25	0.5802(5)	0.7666(6)	0.1309(2)	0.40(7)
O26	0.2409(5)	0.9974(5)	0.4711(2)	0.37(7)
O27	0.5644(5)	0.7830(6)	0.0050(2)	0.44(7)

**TABLE 4**  
**Fractional Atomic Coordinates and Isotropic or Equivalent-Isotropic Displacement Parameters ( $\text{\AA}^2$ ) for  $\text{Nd}_5\text{Mo}_{32}\text{O}_{54}$**

Atom	x	y	z	( $\text{\AA}^2$ )
Nd1	0.000	0.000	0.500	0.54(1)
Nd2	0.22933(6)	-0.00610(8)	0.20481(3)	0.66(1)
Nd3	0.46954(6)	0.00398(8)	0.08067(3)	0.43(1)
Mo1	0.84528(9)	0.1207(1)	0.09597(4)	0.21(1)
Mo2	0.91281(9)	0.6184(1)	0.55163(4)	0.23(1)
Mo3	0.07843(9)	0.1250(1)	0.06835(4)	0.23(1)
Mo4	0.15711(9)	0.8773(1)	0.02131(4)	0.25(1)
Mo5	0.93586(9)	0.8769(1)	0.67697(4)	0.13(1)
Mo6	0.15649(9)	0.8760(1)	0.76675(4)	0.23(1)
Mo7	0.31914(9)	0.1194(1)	0.78836(4)	0.21(1)
Mo8	0.91935(9)	0.8778(1)	0.30312(4)	0.21(1)
Mo9	0.40549(9)	0.8776(1)	0.74201(4)	0.20(1)
Mo10	0.83644(9)	0.1217(1)	0.35041(4)	0.23(1)
Mo11	0.66683(9)	0.8845(1)	0.32935(4)	0.21(1)
Mo12	0.42484(9)	0.8839(1)	0.61297(4)	0.22(1)
Mo13	0.59532(9)	0.1126(1)	0.63027(4)	0.19(1)
Mo14	0.34733(9)	0.1280(1)	0.53836(4)	0.21(1)
Mo15	0.34062(9)	0.1349(1)	0.42517(4)	0.19(1)
Mo16	0.41391(9)	0.8742(1)	0.49051(4)	0.24(1)
O1	0.3333(8)	0.7566(9)	0.9179(4)	0.3(1)
O2	0.2506(7)	0.995(1)	0.8445(3)	0.3(1)
O3	0.0809(8)	0.759(1)	0.8256(4)	0.4(1)
O4	0.8341(7)	0.7471(9)	0.1035(3)	0.2(1)
O5	0.0167(7)	0.993(1)	0.1276(3)	0.3(1)
O6	0.1755(8)	0.2610(9)	0.6501(3)	0.2(1)
O7	0.2701(7)	0.498(1)	0.4761(3)	0.4(1)
O8	0.0776(8)	0.7680(9)	0.4548(4)	0.3(1)
O9	0.9243(8)	0.263(1)	0.9292(4)	0.4(1)
O10	0.2533(8)	0.499(1)	0.5967(3)	0.4(1)
O11	0.8341(8)	0.7383(9)	0.9815(4)	0.4(1)
O12	0.3408(7)	0.7395(9)	0.5460(3)	0.2(1)
O13	0.2459(8)	0.010(1)	0.3485(4)	0.6(1)
O14	0.8341(8)	0.7399(9)	0.2315(4)	0.3(1)
O15	0.0969(7)	0.7719(9)	0.1991(3)	0.1(1)
O16	0.9966(8)	0.989(1)	0.3828(4)	0.4(1)
O17	0.0123(8)	0.992(1)	0.2470(4)	0.6(1)
O18	0.3355(7)	0.7524(9)	0.1679(3)	0.2(1)
O19	0.3236(8)	0.7379(9)	0.7874(4)	0.3(1)
O20	0.4107(8)	0.2481(9)	0.2399(4)	0.3(1)
O21	0.5220(7)	0.996(1)	0.6949(3)	0.2(1)
O22	0.4931(8)	0.999(1)	0.8117(4)	0.6(1)
O23	0.7604(8)	0.997(1)	0.4111(3)	0.3(1)
O24	0.5725(7)	0.7487(9)	0.8831(3)	0.2(1)
O25	0.5783(8)	0.7671(9)	0.1300(4)	0.3(1)
O26	0.2416(7)	0.997(1)	0.4715(3)	0.2(1)
O27	0.5653(8)	0.7821(9)	0.0043(4)	0.4(1)

## RESULTS AND DISCUSSION

All  $\text{RE}_5\text{Mo}_{32}\text{O}_{54}$  compounds are isostructural with  $\text{La}_5\text{Mo}_{32}\text{O}_{54}$  that was briefly described in 1993 by Gall *et al.* (16). Comparison of the unit-cell volumes of the four compounds shows that they decrease regularly from the lanthanum to the neodymium compound as expected from

the lanthanide contraction for  $\text{RE}^{3+}$  cations. These compounds crystallize in the monoclinic  $P2_1/c$  space group. The view of the structure along the *a* axis (Fig. 1) clearly shows that the rare-earths, the oxygen atoms and the molybdenum

**TABLE 5**  
**Selected Mo–Mo Distances ( $\text{\AA}$ ) for  $\text{RE}_5\text{Mo}_{32}\text{O}_{54}$**

	La	Ce	Pr	Nd
Cluster $\text{Mo}_8$				
Mo1–Mo2	2.5728(9)	2.572(2)	2.5750(8)	2.573(2)
Mo1–Mo3	2.6196(9)	2.622(1)	2.6185(8)	2.609(1)
Mo1–Mo4	2.6930(9)	2.688(2)	2.6828(8)	2.674(1)
Mo1–Mo6 <sup>a</sup>	3.1317(9)	3.137(1)	3.1349(8)	3.142(1)
Mo2–Mo4	2.7380(9)	2.737(2)	2.7374(8)	2.737(1)
Mo2–Mo3	2.7484(9)	2.749(2)	2.7487(8)	2.750(1)
Mo2–Mo4	2.7621(8)	2.759(1)	2.7529(8)	2.749(1)
Mo2–Mo3	2.7777(8)	2.775(1)	2.7728(8)	2.767(1)
Mo3–Mo4	2.7061(9)	2.710(2)	2.7088(8)	2.710(1)
Mo3–Mo4	2.7243(9)	2.723(1)	2.7183(8)	2.710(1)
Tricluseter $\text{Mo}_{24}$				
Fragment $\text{Mo}_7$				
Mo5–Mo10	2.5561(9)	2.556(1)	2.5572(8)	2.552(1)
Mo5–Mo6	2.6240(8)	2.622(1)	2.6219(8)	2.610(1)
Mo5–Mo8	2.6494(9)	2.652(2)	2.6490(8)	2.649(1)
Mo5–Mo15 <sup>b</sup>	3.1468(9)	3.149(1)	3.1491(8)	3.147(1)
Mo6–Mo10	2.7068(9)	2.703(1)	2.7045(8)	2.697(1)
Mo6–Mo9	2.7357(9)	2.737(1)	2.7379(8)	2.735(1)
Mo6–Mo7	2.7369(9)	2.734(2)	2.7316(8)	2.733(1)
Mo6–Mo8	2.7463(9)	2.744(2)	2.7445(8)	2.744(1)
Mo7–Mo9	2.6945(9)	2.690(2)	2.6891(8)	2.691(1)
Mo7–Mo11	2.7313(9)	2.734(1)	2.7368(8)	2.731(1)
Mo7–Mo8	2.7564(9)	2.757(1)	2.7578(8)	2.753(1)
Mo8–Mo10	2.7037(9)	2.704(2)	2.7001(8)	2.702(1)
Mo8–Mo11	2.7925(8)	2.791(1)	2.7913(8)	2.786(1)
Mo9–Mo11	2.6978(9)	2.693(2)	2.6956(8)	2.697(1)
Mo9–Mo10	2.7913(9)	2.790(1)	2.7906(8)	2.788(1)
Mo9–Mo12 <sup>c</sup>	3.0053(9)	3.010(1)	3.0069(8)	3.008(1)
Mo10–Mo11	2.7322(9)	2.732(2)	2.7274(8)	2.728(1)
Mo10–Mo12 <sup>c</sup>	2.9916(9)	2.995(1)	2.9896(8)	2.988(1)
Mo11–Mo12 <sup>c</sup>	2.7688(9)	2.772(2)	2.7704(8)	2.777(1)
Mo11–Mo13 <sup>c</sup>	3.0373(9)	3.043(1)	3.0399(8)	3.041(1)
Mo11–Mo14 <sup>c</sup>	3.0637(9)	3.067(1)	3.0628(8)	3.067(1)
Fragment $\text{Mo}_{10}$				
Mo12–Mo13	2.6736(9)	2.674(2)	2.6731(8)	2.673(1)
Mo12–Mo15	2.7531(8)	2.787(2)	2.7557(8)	2.751(1)
Mo12–Mo16	2.7755(9)	2.754(1)	2.7756(8)	2.773(1)
Mo12–Mo14	2.7908(9)	2.776(1)	2.7844(8)	2.787(1)
Mo13–Mo15	2.7421(9)	2.746(2)	2.7463(8)	2.749(1)
Mo13–Mo16	2.7474(9)	2.745(1)	2.7441(8)	2.740(1)
Mo13–Mo14	2.8308(8)	2.832(1)	2.8303(8)	2.828(1)
Mo14–Mo15	2.5879(9)	2.585(1)	2.5809(8)	2.570(1)
Mo14–Mo16	2.6839(9)	2.717(2)	2.6845(8)	2.678(1)
Mo14–Mo16	2.7152(9)	2.687(1)	2.7147(8)	2.719(1)
Mo15–Mo16	2.7351(9)	2.734(1)	2.7301(8)	2.722(1)
Mo15–Mo16	2.8013(9)	2.800(2)	2.7986(8)	2.801(1)
Mo16–Mo16	2.838(1)	2.841(2)	2.840(1)	2.848(2)

<sup>a</sup>Between the  $\text{Mo}_8$  cluster and the  $\text{Mo}_7$  of the tricluseter.

<sup>b</sup>Between the  $\text{Mo}_7$  and  $\text{Mo}_{10}$  clusters of different tricluseter.

<sup>c</sup>Between the  $\text{Mo}_7$  and  $\text{Mo}_{10}$  clusters of the same tricluseter.

**TABLE 6**  
Selected Mo–O Distances (Å) for  $\text{RE}_5\text{Mo}_{32}\text{O}_{54}$

	La	Ce	Pr	Nd
Cluster $\text{Mo}_8$				
Mo1–O3	2.045(5)	2.048(9)	2.042(5)	2.065(9)
Mo1–O5	2.061(5)	2.069(9)	2.056(5)	2.060(8)
Mo1–O8	2.075(5)	2.07(1)	2.082(5)	2.060(8)
Mo1–O7	2.089(5)	2.080(8)	2.086(5)	2.081(8)
Mo1–O1	2.097(5)	2.107(9)	2.090(5)	2.084(8)
Mo1–O2	2.148(5)	2.139(9)	2.134(5)	2.149(8)
Mo2–O4	2.019(5)	2.024(9)	2.021(5)	2.012(8)
Mo2–O5	2.051(5)	2.051(8)	2.061(5)	2.050(8)
Mo2–O11	2.063(5)	2.062(9)	2.046(5)	2.058(9)
Mo2–O9	2.075(5)	2.081(9)	2.073(5)	2.068(8)
Mo2–O7	2.105(5)	2.107(8)	2.097(5)	2.087(8)
Mo3–O5	2.031(5)	2.043(9)	2.035(5)	2.029(8)
Mo3–O8	2.033(5)	2.012(9)	2.028(5)	2.013(8)
Mo3–O11	2.039(5)	2.043(9)	2.056(5)	2.044(8)
Mo3–O10	2.060(5)	2.050(9)	2.053(5)	2.061(8)
Mo3–O6	2.131(5)	2.135(9)	2.128(5)	2.138(8)
Mo4–O9	2.027(5)	2.051(9)	2.027(5)	2.021(9)
Mo4–O8	2.033(5)	2.03(1)	2.034(5)	2.018(8)
Mo4–O10	2.076(5)	2.076(9)	2.067(5)	2.076(8)
Mo4–O7	2.080(5)	2.068(9)	2.071(5)	2.077(8)
Mo4–O12	2.101(5)	2.091(8)	2.104(5)	2.094(8)
Tricluseter $\text{Mo}_{24}$				
Fragment $\text{Mo}_7$				
Mo5–O17	2.053(5)	2.045(8)	2.055(5)	2.062(9)
Mo5–O16	2.063(5)	2.057(9)	2.055(5)	2.078(9)
Mo5–O15	2.071(5)	2.062(9)	2.090(5)	2.083(8)
Mo5–O4	2.073(5)	2.066(9)	2.062(5)	2.061(8)
Mo5–O13	2.073(5)	2.070(9)	2.075(5)	2.061(9)
Mo5–O14	2.092(5)	2.121(9)	2.088(5)	2.106(8)
Mo6–O15	2.029(5)	2.028(9)	2.031(5)	2.019(8)
Mo6–O3	2.031(5)	2.023(9)	2.028(5)	2.020(9)
Mo6–O17	2.062(5)	2.071(8)	2.059(5)	2.053(9)
Mo6–O19	2.087(5)	2.063(9)	2.073(5)	2.067(8)
Mo6–O2	2.096(5)	2.091(9)	2.099(5)	2.088(8)
Mo7–O2	1.983(5)	1.986(9)	1.985(5)	1.970(8)
Mo7–O14	1.984(5)	1.966(9)	1.989(5)	1.976(8)
Mo7–O20	2.027(5)	2.030(9)	2.030(5)	2.024(8)
Mo7–O22	2.050(5)	2.024(9)	2.032(5)	2.028(9)
Mo7–O25	2.140(5)	2.136(9)	2.135(5)	2.149(9)
Mo8–O3	2.034(5)	2.038(9)	2.039(5)	2.019(9)
Mo8–O17	2.055(5)	2.074(8)	2.065(5)	2.061(9)
Mo8–O16	2.058(5)	2.057(9)	2.055(5)	2.053(8)
Mo8–O6	2.061(5)	2.049(9)	2.056(5)	2.054(8)
Mo8–O14	2.084(5)	2.066(9)	2.083(5)	2.065(8)
Mo9–O22	1.957(5)	1.961(9)	1.942(5)	1.953(9)
Mo9–O19	1.975(5)	1.978(9)	1.968(5)	1.961(8)
Mo9–O18	2.017(5)	2.024(9)	2.019(5)	2.035(8)
Mo9–O21	2.111(5)	2.104(9)	2.104(5)	2.098(8)
Mo9–O20	2.139(5)	2.141(8)	2.141(5)	2.137(8)
Mo10–O16	2.005(5)	2.002(9)	1.994(5)	2.004(8)
Mo10–O15	2.007(5)	1.994(9)	2.023(5)	2.005(8)
Mo10–O18	2.018(5)	2.014(9)	2.081(5)	2.065(8)
Mo10–O9	2.079(5)	2.061(9)	2.076(5)	2.075(9)
Mo10–O23	2.117(5)	2.112(9)	2.114(5)	2.092(8)
Mo11–O20	2.022(5)	2.010(9)	2.004(5)	2.002(9)
Mo11–O6	2.051(5)	2.053(9)	2.054(5)	2.037(8)

**TABLE 6—Continued**

	La	Ce	Pr	Nd
Tricluseter $\text{Mo}_{24}$				
Fragment $\text{Mo}_7$				
Mo11–O24	2.112(5)	2.110(9)	2.125(5)	2.126(8)
Mo11–O23	2.119(5)	2.126(8)	2.128(5)	2.125(8)
Mo11–O21	2.139(5)	2.145(9)	2.132(5)	2.149(8)
Fragment $\text{Mo}_{10}$				
Mo12–O12	2.034(5)	2.032(8)	2.024(5)	2.028(8)
Mo12–O25	2.047(5)	2.072(9)	2.055(5)	2.040(8)
Mo12–O23	2.106(5)	2.111(8)	2.107(5)	2.116(8)
Mo12–O18	2.129(5)	2.118(9)	2.134(5)	2.133(8)
Mo12–O21	2.142(5)	2.129(9)	2.133(5)	2.134(8)
Mo13–O13	1.919(5)	1.923(9)	1.912(5)	1.917(9)
Mo13–O1	1.958(5)	1.943(9)	1.958(5)	1.970(8)
Mo13–O24	2.048(5)	2.036(9)	2.053(5)	2.065(8)
Mo13–O21	2.098(5)	2.104(9)	2.100(5)	2.108(8)
Mo13–O19	2.160(5)	2.163(9)	2.165(5)	2.170(8)
Mo14–O26	2.029(5)	2.030(9)	2.019(5)	2.012(8)
Mo14–O11	2.053(5)	2.046(8)	2.055(5)	2.044(8)
Mo14–O27	2.060(5)	2.070(9)	2.069(5)	2.042(9)
Mo14–O24	2.075(5)	2.063(9)	2.072(5)	2.080(8)
Mo14–O23	2.100(5)	2.108(9)	2.097(5)	2.121(8)
Mo15–O4	2.011(5)	2.012(9)	2.007(5)	2.004(8)
Mo15–O26	2.059(5)	2.087(9)	2.064(5)	2.069(8)
Mo15–O25	2.069(5)	2.054(9)	2.070(5)	2.065(8)
Mo15–O13	2.097(5)	2.105(9)	2.099(5)	2.099(9)
Mo15–O27	2.124(5)	2.128(9)	2.128(5)	2.121(9)
Mo16–O12	2.036(5)	2.041(8)	2.041(5)	2.042(8)
Mo16–O26	2.045(5)	2.026(9)	2.035(5)	2.026(8)
Mo16–O1	2.058(5)	2.038(9)	2.049(5)	2.032(8)
Mo16–O27	2.071(5)	2.061(9)	2.063(5)	2.060(8)

clusters are arranged in layers parallel to the *ac* plane. The oxygen atom network can thus be described as a stacking of compact layers with a  $|ABAC|A\dots$  sequence (Fig. 2). Contrary to the *B* ( $y \approx 0.25$ ) and *C* ( $y \approx 0.75$ ) layers that are fully occupied with oxygen atoms and can thus be formulated  $[\text{O}_{32}]$ , the *A* ( $y \approx 0.0$  and  $y \approx 0.5$ ) layers exhibit vacancies. In comparison with a fully occupied layer of 32 oxygen atoms, 10 of them are missing and half of the latter are replaced by rare-earths, the result of which is a mixed *A* layer of formula  $[\text{O}_{22}\text{RE}_5\square_5]$  ( $\square$  symbolizes a vacancy). Within this oxygen network, all tetrahedral sites are empty and half of the octahedral sites are occupied by the molybdenum atoms that form the  $\text{Mo}_8$  and  $\text{Mo}_{24}$  clusters. A projected view of the metallic network on the (*ac*) plane is presented in Fig. 3. Both clusters are shown in Fig. 4 with their oxygen environment. While the bicapped  $\text{Mo}_8$  cluster, having here the *trans* configuration, has previously been observed in the polymorphic compounds  $\text{REMo}_8\text{O}_{14}$  [La (25–27), Ce (28), Pr (29), Nd (30), Sm (31)], the isolated  $\text{Mo}_{24}$  cluster is unprecedented. It results from the interconnection of one bioctahedral  $\text{Mo}_{10}$  cluster with two monocapped octahedral  $\text{Mo}_7$  clusters in a manner similar to that

**TABLE 7**  
Selected RE–O Distances ( $\text{\AA}$ ) for  $\text{RE}_5\text{Mo}_{32}\text{O}_{54}$

	La	Ce	Pr	Nd
$\text{RE1-O8} (\times 2)$	2.572(5)	2.57(1)	2.551(5)	2.567(9)
$\text{RE1-O16} (\times 2)$	2.689(5)	2.693(8)	2.690(5)	2.670(8)
$\text{RE1-O26} (\times 2)$	2.699(5)	2.697(8)	2.702(5)	2.702(8)
$\text{RE1-O9} (\times 2)$	2.721(5)	2.698(9)	2.693(5)	2.691(9)
$\text{RE1-O11} (\times 2)$	2.741(5)	2.736(8)	2.711(5)	2.714(8)
$\text{RE1-O23} (\times 2)$	2.748(5)	2.741(8)	2.740(5)	2.730(8)
$\text{RE2-O5}$	2.477(5)	2.442(8)	2.424(5)	2.403(8)
$\text{RE2-O15}$	2.487(5)	2.470(9)	2.425(5)	2.415(8)
$\text{RE2-O10}$	2.582(5)	2.571(8)	2.562(5)	2.547(8)
$\text{RE2-O6}$	2.596(5)	2.579(9)	2.561(5)	2.548(9)
$\text{RE2-O17}$	2.666(5)	2.635(8)	2.639(5)	2.631(8)
$\text{RE2-O18}$	2.708(5)	2.716(9)	2.693(5)	2.683(8)
$\text{RE2-O19}$	2.835(5)	2.850(9)	2.832(5)	2.827(9)
$\text{RE2-O14}$	2.837(5)	2.834(9)	2.840(5)	2.839(9)
$\text{RE2-O22}$	2.873(5)	2.917(8)	2.930(5)	2.944(8)
$\text{RE2-O21}$	2.879(5)	2.911(8)	2.931(5)	2.932(8)
$\text{RE2-O20}$	2.888(5)	2.914(9)	2.922(5)	2.938(8)
$\text{RE2-O13}$	3.206(5)	3.215(8)	3.236(5)	3.247(8)
$\text{RE3-O10}$	2.405(5)	2.382(8)	2.358(5)	2.322(8)
$\text{RE3-O22}$	2.441(5)	2.422(8)	2.414(5)	2.387(8)
$\text{RE3-O24}$	2.536(5)	2.533(9)	2.495(5)	2.478(8)
$\text{RE3-O25}$	2.593(5)	2.579(9)	2.565(5)	2.549(9)
$\text{RE3-O12}$	2.653(5)	2.642(9)	2.610(5)	2.592(8)
$\text{RE3-O27}$	2.726(5)	2.717(9)	2.712(5)	2.709(9)
$\text{RE3-O7}$	2.738(5)	2.721(8)	2.709(5)	2.696(8)
$\text{RE3-O2}$	2.847(5)	2.876(8)	2.896(5)	2.908(8)
$\text{RE3-O1}$	2.905(5)	2.943(9)	2.942(5)	2.958(8)
$\text{RE3-O27}$	2.947(5)	2.955(9)	2.966(5)	2.996(9)
$\text{RE3-O7}$	3.142(5)	3.188(8)	3.220(5)	3.240(8)

encountered in the step-stair chains based on  $\text{Mo}_{10}$  clusters occurring in the series of compounds  $\text{MMo}_5\text{O}_8$  (10). It is interesting to mention that the oxygen vacancies of the  $A$  layers correspond to the centers of the  $\text{Mo}_6$  octahedral

**TABLE 8**  
Resistivity Data for the  $\text{RE}_5\text{Mo}_{32}\text{O}_{54}$  ( $\text{RE} = \text{La, Ce, Pr, Nd}$ ) Compounds

	Crystal dimensions ( $\text{mm}^3$ )	$\rho_{293}$ ( $\Omega \cdot \text{cm}$ )	$E_a$ (eV)
$\text{La}_5\text{Mo}_{32}\text{O}_{54}$	$0.10 \times 0.20 \times 0.58$	0.041	0.070
$\text{Ce}_5\text{Mo}_{32}\text{O}_{54}$	$0.08 \times 0.24 \times 0.68$	0.076	0.058
$\text{Pr}_5\text{Mo}_{32}\text{O}_{54}$	$0.14 \times 0.22 \times 0.52$	0.045	0.066
$\text{Nd}_5\text{Mo}_{32}\text{O}_{54}$	$0.14 \times 0.24 \times 0.50$	0.039	0.065

core of the  $\text{Mo}_8$  and  $\text{Mo}_{24}$  clusters. The oxygen atoms bridge all Mo–Mo edges or are linked to free apices. The  $\text{Mo}_8$  cluster and the  $\text{Mo}_{24}$  trilcluster are surrounded by 24 and 60 oxygen atoms, respectively, as represented in Fig. 4. Within the  $\text{Mo}_8$  cluster, the Mo–Mo distances lie between 2.57 and 2.72  $\text{\AA}$  with average values of 2.705, 2.704, 2.702, and 2.698  $\text{\AA}$  for the La, Ce, Pr, and Nd, respectively. The latter values are similar to those found for the  $\text{RMo}_8\text{O}_{14}$  compounds in which trans  $\text{Mo}_8$  clusters are present (27–29). The slight decrease when going from lanthanum to neodymium arises probably from some sterical effects due to the lanthanide contraction. In the  $\text{Mo}_{24}$  chain-fragment, the Mo–Mo distances are between 2.55 and 2.79  $\text{\AA}$  (average values 2.710, 2.709, 2.709, and 2.706  $\text{\AA}$  for the La, Ce, Pr, and Nd compounds, respectively) within the  $\text{Mo}_7$  fragment and between 2.57 and 2.84  $\text{\AA}$  (average values 2.740, 2.740, 2.739, and 2.737  $\text{\AA}$  for the La, Ce, Pr, and Nd compounds, respectively) for the  $\text{Mo}_{10}$  fragment. The shortest Mo–Mo distance between the  $\text{Mo}_7$  and the  $\text{Mo}_{10}$  fragments is 2.77  $\text{\AA}$  ( $\text{Mo11–Mo12}$ ). The shortest Mo–Mo distances within the same layer between the quasi-isolated clusters are about 3.13  $\text{\AA}$  ( $\text{Mo1–Mo6}$ ) between the  $\text{Mo}_8$  cluster and the  $\text{Mo}_7$  fragment of the trilcluster and about 3.15  $\text{\AA}$  ( $\text{Mo5–Mo15}$ )

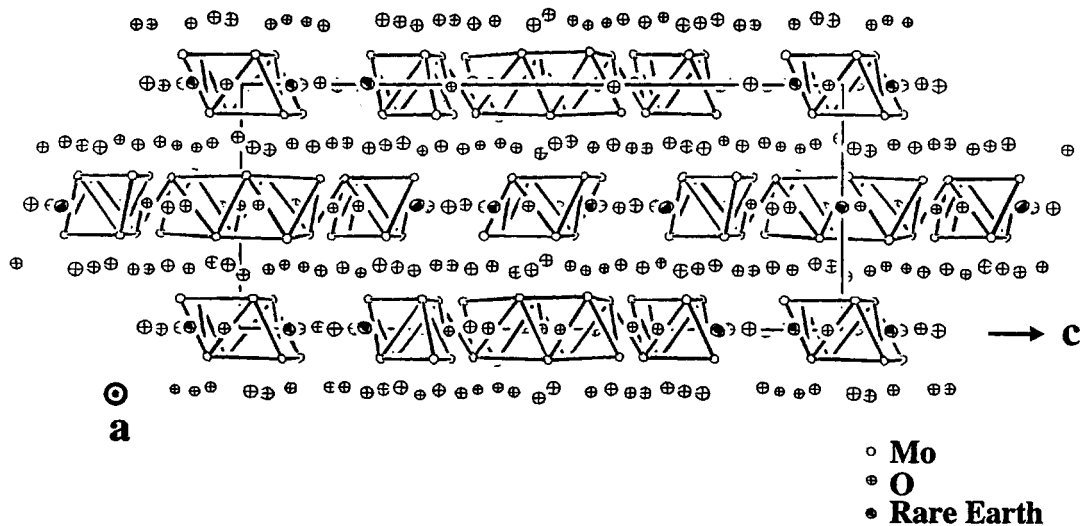


**FIG. 1.** Projected view of the structure along the  $a$  axis.

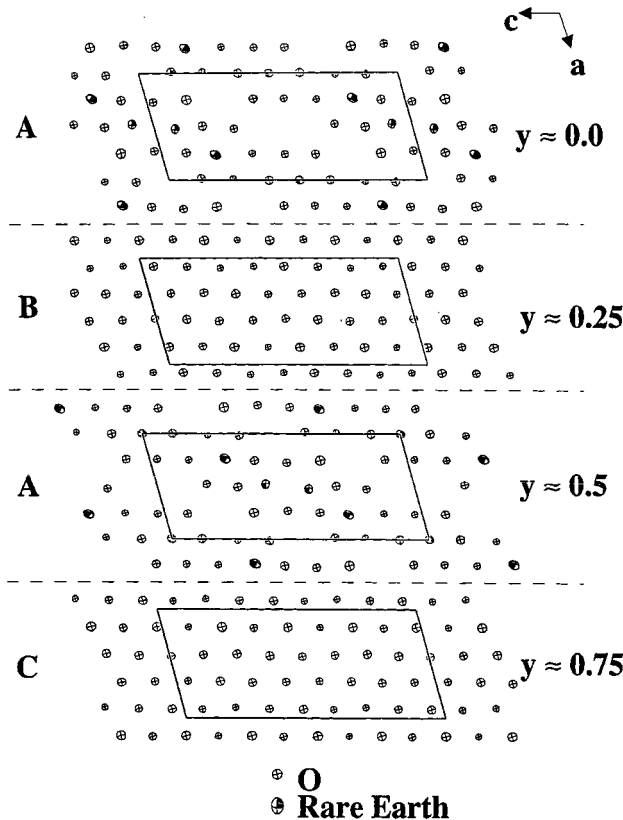


FIG. 2. *ABAC* arrangement of the oxygen–rare earth layers.

between the  $\text{Mo}_7$  fragment and the  $\text{Mo}_{10}$  fragment of different triclusters. Between different metallic layers, the shortest Mo–Mo distance is observed between the  $\text{Mo}_8$  cluster and the  $\text{Mo}_{10}$  fragment of the tricuster and is about 3.58 Å

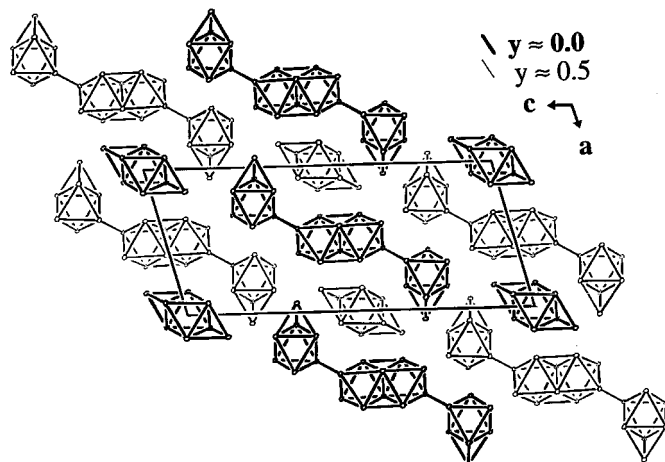
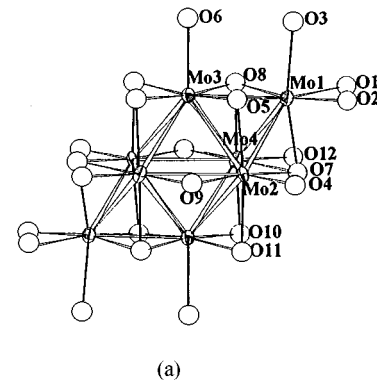
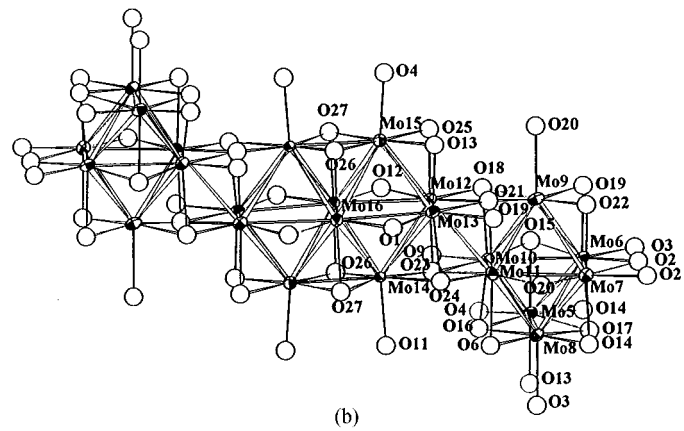


FIG. 3. Projection of the molybdenum network of  $\text{La}_5\text{Mo}_{32}\text{O}_{54}$  onto the *ac* plane. Clusters represented in thick lines are at level  $y \approx 0.0$  and those in thin lines are at level  $y \approx 0.5$ . Only Mo–Mo bonds less than 2.9 Å are represented.



(a)



(b)

FIG. 4. (a) The  $\text{Mo}_8$  cluster and (b) the  $\text{Mo}_7\text{–Mo}_{10}\text{–Mo}_7$  tricuster with their oxygen environment.

( $\text{Mo}2\text{–Mo}15$ ). Consequently, although the structure is three-dimensional overall, it can be considered to be two-dimensional with respect to the Mo network. The Mo–O bond distances are in the range 1.91–2.17 Å with an average value of 2.06 Å for the  $\text{Mo}_{24}\text{O}_{60}$  unit, and in the range 2.01–2.15 Å with an average value of 2.06 Å for the  $\text{Mo}_8\text{O}_{24}$  unit.

The  $\text{RE}^{3+}$  ions are located in the anionic layers at the levels  $y \approx 0.0$  and  $y \approx 0.5$ . Of the three crystallographically independent  $\text{RE}^{3+}$  ions, two of them ( $\text{RE}1$  and  $\text{RE}2$ ) are surrounded by 12 oxygen atoms forming a distorted cube-octahedron (Fig. 5a) and the third ( $\text{RE}3$ ) rare-earth cation occupies large cavities that result from the fusion of two cube-octahedra and is thus surrounded by 11 oxygen atoms (Fig. 5b). The RE–O distances range from 2.55 to 3.24 Å with an average value of 2.72 Å for the La and Ce compounds and 2.71 Å for the Pr and Nd compounds.

The temperature dependencies of the electrical resistivities measured in the *ac* plane show that all  $\text{RE}_5\text{Mo}_{32}\text{O}_{54}$  compounds ( $\text{RE} = \text{La}, \text{Ce}, \text{Pr}, \text{Nd}$ ) are semiconductors in the temperature range 80–290 K (Fig. 6) with a small activation energy of about 0.06 eV. The  $\log(\rho)$  vs  $1000/T$  plots show a quasi-linear variation that is characteristic of semiconducting compounds that can be described by the

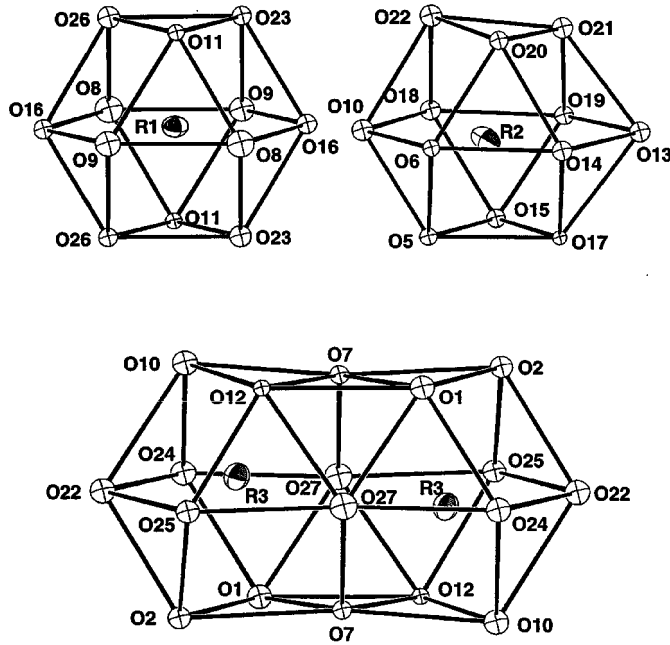


FIG. 5. Environments of the rare-earths in the  $RE_5Mo_{32}O_{54}$  compounds.

activation law:  $\log(\rho) = -Ea/2.3 k_B T$ . The crystal dimensions, the room temperature resistivities, and calculated activation energies are given in Table 8. This semiconducting behavior can be attributed to the shortest intercluster distance of 3.13 Å which is relatively long. For example, the family of compounds  $REMo_8O_{14}$  ( $RE = La, Ce, Pr, Nd$ , or Sm) presents intercluster distances of about 3.07 Å and

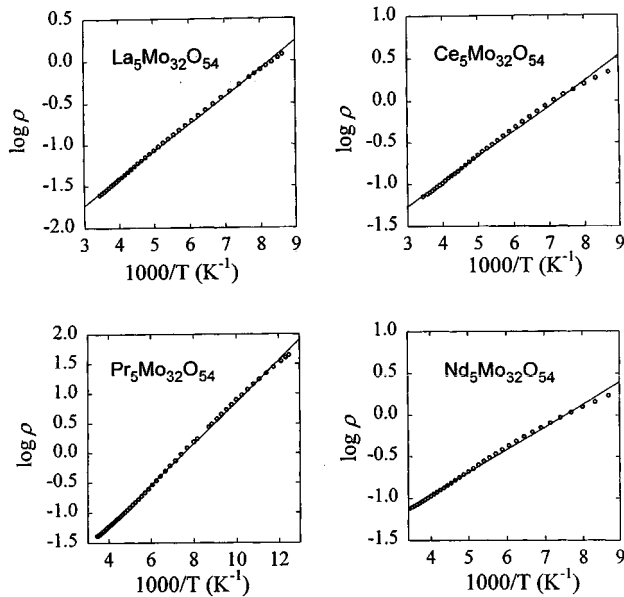


FIG. 6. Arrhenius plots for the  $RE_5Mo_{32}O_{54}$  compounds.

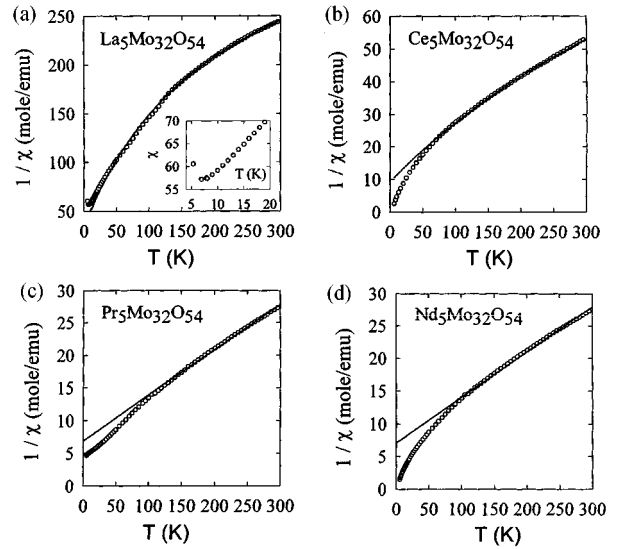


FIG. 7. (a) Inverse magnetic susceptibility vs temperature for  $La_5Mo_{32}O_{54}$ . (Inset) Susceptibility vs temperature at low temperature. Inverse magnetic susceptibility vs temperature for (b)  $Ce_5Mo_{32}O_{54}$ , (c)  $Pr_5Mo_{32}O_{54}$ , and (d)  $Nd_5Mo_{32}O_{54}$ .

shows semiconducting behavior with ambient resistivities of a similar magnitude. The  $Ba_3Mo_{18}O_{28}$  compound (12) also presents semiconducting behavior with a shortest intercluster distance of about 3.17 Å.

A plot of the inverse of the magnetic susceptibility of  $La_5Mo_{32}O_{54}$  is shown in Fig. 7a.  $La_5Mo_{32}O_{54}$  presents temperature-dependent paramagnetic behavior. The data can be least-squares fit to a modified Curie-Weiss law  $\chi = C/(T - \theta) + \chi_0$  over the temperature range 140–300 K giving an effective magnetic moment  $\mu_{eff} = 1.77 \mu_B$ . As the  $La^{3+}$  ion is nonmagnetic, this moment can be attributed only to a magnetic moment arising from the molybdenum clusters. The value of  $1.77 \mu_B$  corresponds approximately to one electron per formula ( $RE_5Mo_{32}O_{54}$ ) localized on the molybdenum clusters ( $Mo_8 + Mo_{24}$ ). Magnetic measurement and theoretical studies were recently made on the  $LaMo_8O_{14}$  compound which contains *cis* and *trans*  $Mo_8$  clusters in equal proportion (32). These show that  $LaMo_8O_{14}$  presents temperature independent paramagnetic behavior with  $24e^-$  per *trans*  $Mo_8$  cluster and  $22e^-$  per *cis*  $Mo_8$  cluster. As the Mo-Mo distances within the *trans*  $Mo_8$  clusters present in  $La_5Mo_{32}O_{54}$  and  $LaMo_8O_{14}$  are similar, we can also expect  $24e^-$  per  $Mo_8$  cluster and thus that the magnetic moment observed in  $La_5Mo_{32}O_{54}$  probably arises from the  $Mo_7-Mo_{10}-Mo_7$  tricluster containing  $75e^-$ . The insert also shows a minimum of the inverse susceptibility at about 7 K that suggests an antiferromagnetic ordering between the molybdenum triclusters. The plots  $1/\chi = f(T)$  for the  $Ce_5Mo_{32}O_{54}$ ,  $Pr_5Mo_{32}O_{54}$ , and  $Nd_5Mo_{32}O_{54}$  compounds are presented in Figs. 7b, 7c, and 7d, respectively. They show paramagnetic behavior for

**TABLE 9**  
**Magnetic Susceptibility Data for the  $RE_5Mo_{32}O_{54}$**   
**( $RE = La, Ce, Pr, Nd$ ) Compounds**

	$La_5Mo_{32}O_{54}$	$Ce_5Mo_{32}O_{54}$	$Pr_5Mo_{32}O_{54}$	$Nd_5Mo_{32}O_{54}$
$T_1-T_2$ (K)	140–300	80–300	120–300	80–300
$\mu_{eff}$ ( $\mu_B$ )	1.77	2.67	3.77	3.76
$\mu_{RE}$ ( $\mu_B$ )	—	2.52	3.67	3.66
$\mu_{Free\ ion}$ ( $\mu_B$ )	0	2.54	3.58	3.62
$\theta_p$ (K)	–11.9	–46.4	–35.9	–42.6
$\chi_0$ ( $10^{-3}$ emu/mol)	2.578	5.947	9.882	10.622

the latter three compounds in the whole range of temperature. The fact that the effective moments ( $\mu_{eff}$ ) calculated from the modified Curie–Weiss law are all greater than the theoretical moments of the  $RE^{3+}$  free ions ( $\mu_{Free\ ion}$ ) confirms the presence of paramagnetism due to localized electrons on the molybdenum clusters in addition to the paramagnetism of the  $4f$  electrons of lanthanide ions. The effective moments of the rare-earth ions ( $\mu_{RE}$ ) can be obtained by subtracting the magnetic contribution of the metallic network obtained for  $La_5Mo_{32}O_{54}$  from the observed values for the Ce, Pr, and Nd compounds. The resulting  $\mu_{RE}$  values are in good agreement with the theoretical moments calculated for the  $RE^{3+}$  free ions ( $\mu_{Free\ ion}$ ). All magnetic data are summarized in Table 9.

In summary, compounds isostructural with  $La_5Mo_{32}O_{54}$ , that was first described in 1993 by Gall *et al.* (6), have been synthesized with cerium, praseodymium, and neodymium. Electrical and magnetic properties have been investigated for the whole family of compounds. The resistivity measurements show that the four isostructural compounds exhibit similar semiconducting behavior with a small activation energy of about 0.06 at high temperature. The magnetic data reveal the existence of a magnetic moment of  $1.77\ \mu_B$  that corresponds to one unpaired electron per  $RE_5Mo_{32}O_{54}$  formula localized on the molybdenum clusters, in addition to the paramagnetism of the trivalent rare-earth cations.

## REFERENCES

- P. Gougeon, J. Padiou, J. Y. Le Marouille, M. Potel, and M. Sergent, *J. Solid State Chem.* **51**, 218 (1984).
- P. Gougeon, M. Potel, J. Padiou, and M. Sergent, *Mater. Res. Bull.* **22**, 1087 (1988).
- P. Gougeon, M. Potel, and M. Sergent, *Acta Crystallogr. C* **45**, 182 (1989); P. Gougeon, M. Potel, and M. Sergent, *Acta Crystallogr. C* **45**, 1413 (1989).
- P. Gougeon, M. Potel, J. Padiou, and M. Sergent, *Mater. Res. Bull.* **23**, 453 (1988).
- P. Gougeon, M. Potel, and M. Sergent, *Acta Crystallogr. C* **46**, 2284 (1990); S. Picard, P. Gougeon, and M. Potel, *Acta Crystallogr. C* **53**, 1519 (1997).
- P. Gougeon, *Thesis*, Rennes, 1984.
- S. Picard, M. Potel, and P. Gougeon, *Angew. Chem.* **38**, 2023 (1999).
- M. Potel, *Thesis*, Rennes, 1984.
- P. Gougeon, M. Potel, J. Padiou, and M. Sergent, *J. Solid State Chem.* **68**, 137 (1987).
- S. J. Hibble, A. K. Cheetham, A. R. L. Bogle, H. R. Wakerley, and D. E. Cox, *J. Am. Chem. Soc.* **110**, 3295 (1988); R. Dronskowski and A. Simon, *Angew. Chem.* **101**, 775 (1989); P. Gougeon, M. Potel, and M. Sergent, *Acta Crystallogr. C* **46**, 1188 (1990); P. Gougeon, P. Gall, and M. Sergent, *Acta Crystallogr. C* **47**, 421 (1991); R. Dronskowski, A. Simon, and W. Z. Mertin, *Z. Anorg. Allg. Chem.* **602**, 49 (1991); P. Gougeon and P. Gall, *Acta Crystallogr. C* **50**, 7 (1994); P. Gougeon and P. Gall, *Acta Crystallogr. C* **50**, 1183 (1994).
- R. Dronskowski, A. Simon, and W. Z. Mertin, *Anorg. Allg. Chem.* **602**, 49 (1991); R. Dronskowski and A. Simon, *Acta Chem. Scand.* **45**, 850 (1991); G. L. Schimek, S. C. Chen, and R. E. McCarley, *Inorg. Chem.* **34**, 6130 (1995).
- G. L. Schimek, D. A. Nagaki, and R. E. McCarley, *Inorg. Chem.* **33**, 1259 (1994); E. Fais, H. Borrman, H. Mattausch, and A. Simon, *Zeit. Anorg. Allg. Chem.* **621**, 1178 (1995).
- R. Dronskowski, H. J. Mattausch, and A. Simon, *Zeit. Anorg. Allg. Chem.* **619**, 1397 (1993); G. L. Schimek and R. E. McCarley, *J. Solid State Chem.* **113**, 345 (1994).
- C. C. Torardi and R. E. McCarley, *J. Am. Chem. Soc.* **101**, 3963 (1979).
- J. Tortelier and P. Gougeon, *Inorg. Chem.* **37**, 6229 (1998).
- P. Gall, L. Toupet, and P. Gougeon, *Acta Crystallogr. C* **49**, 1580 (1993).
- J. Tortelier and P. Gougeon, *Acta Crystallogr. C* **52**, 1862 (1996).
- J. Tortelier, P. Gougeon, K. V. Ramanujachary, and M. Greenblatt, *Mater. Res. Bull.* **33**, 1151 (1998).
- R. Brusetti, P. Monceau, M. Potel, P. Gougeon, and M. Sergent, *Solid State Commun.* **66**, 181 (1988); R. Brusetti, O. Laborde, A. Sulpice, R. Calemczuk, M. Potel, and P. Gougeon, *Phys. Rev. B* **52**, 4481 (1995).
- K. V. Ramanujachary, M. Greenblatt, E. B. Jones, and W. H. McCarroll, *J. Solid State Chem.* **102**, 69 (1993); P. Gall, P. Gougeon, M. Greenblatt, W. H. McCarroll, and K. V. Ramanujachary, *J. Solid State Chem.* **134**, 45 (1997).
- B. T. Collins, M. Greenblatt, W. H. McCarroll, and G. W. Hull, *J. Solid State Chem.* **73**, 507 (1988); K. V. Ramanujachary, M. Greenblatt, W. H. McCarroll, and J. B. Goodenough, *Mater. Res. Bull.* **28**, 1257 (1993); P. Gall, P. Gougeon, M. Greenblatt, E. B. Jones, W. H. McCarroll, and K. V. Ramanujachary, *Croat. Chem. Acta* **68**, 849 (1995).
- P. Gall, H. Noël, and P. Gougeon, *Mater. Res. Bull.* **28**, 1225 (1993).
- A. C. T. North, D. C. Phillips, and F. S. Mathews, *Acta Crystallogr. A* **24**, 351 (1968).
- C. K. Fair, “Mo1EN User’s Manual. An Interactive Intelligent System For Crystal Structure Analysis.” Enraf-Nonius, Delft, The Netherlands, 1989.
- H. Leligny, M. Ledésert, P. Labbé, B. Raveau, and W. H. McCarroll, *J. Solid State Chem.* **87**, 35 (1990).
- H. Leligny, P. Labbé, M. Ledésert, M. Hervieu, B. Raveau, and W. H. McCarroll, *Acta Crystallogr. B* **49**, 444 (1993).
- G. Kerihuel, J. Tortelier, and P. Gougeon, *Acta Crystallogr. C* **52**, 2389 (1996).
- G. Kerihuel and P. Gougeon, *Acta Crystallogr. C* **51**, 787 (1995).
- G. Kerihuel and P. Gougeon, *Acta Crystallogr. C* **51**, 1475 (1995).
- P. Gougeon and R. E. McCarley, *Acta Crystallogr. C* **47**, 241 (1991).
- J. Tortelier and P. Gougeon, *Acta Crystallogr. C* **53**, 668 (1997).
- R. Gautier and P. Gougeon, to be published.